Accepted Manuscript

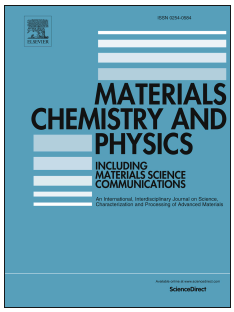

A DFT + U and *ab initio* atomistic thermodynamics approaches for mixed transitional metallic oxides: A case study of $CoCu_2O_3$ surface terminations

Hantarto Widjaja, Hussein Miran, Mohammednoor Altarawneh, Ibukun Oluwoye, Hong Ngee Lim, Nay Ming Huang, Zhong-Tao Jiang, Bogdan Z. Dlugogorski

PII: S0254-0584(17)30663-6

DOI: 10.1016/j.matchemphys.2017.08.047

Reference: MAC 19945

To appear in: *Materials Chemistry and Physics*

Received Date: 22 April 2017

Revised Date: 23 July 2017

Accepted Date: 17 August 2017

Please cite this article as: H. Widjaja, H. Miran, M. Altarawneh, I. Oluwoye, H.N. Lim, N.M. Huang, Z.-T. Jiang, B.Z. Dlugogorski, A DFT + U and *ab initio* atomistic thermodynamics approaches for mixed transitional metallic oxides: A case study of $CoCu_2O_3$ surface terminations, *Materials Chemistry and Physics* (2017), doi: 10.1016/j.matchemphys.2017.08.047.

A DFT + U and ab initio Atomistic Thermodynamics Approaches for Mixed Transitional Metallic Oxides: A Case Study of $CoCu_2O_3$ Surface Terminations

Hantarto Widjaja[a], Hussein Miran[a], Mohammednoor Altarawneh[a]*, Ibukun Oluwoye[a], Hong Ngee Lim,[b] Nay Ming Huang,[c] Zhong-Tao Jiang[a], Bogdan Z. Dlugogorski[a]

[a] School of Engineering and Information Technology, Murdoch University, WA 6150, Australia

[b] Department of Chemistry, Faculty of Science, Universiti Putra Malaysia, 43400 UPM Serdang, Selangor, Malaysia

[c]Faculty of Engineering, Xiamen University of Malaysia, Jalan Sunsuria, Bandar Sunsuria, 43900 Sepang, Selangor Darul Ehsan, Malaysia

*Corresponding Authors:

Phone: (+61) 8 9360-7507

E-mail: M.Altarawneh@Murdoch.edu.au

Abstract

This study develops a systematic density functional theory alongside on-site Coulomb interaction correction (DFT+U) and *ab initio* atomistic thermodynamics approachs for ternary (or mixed transitional metal oxides), expressed in three reservoirs. As a case study, among notable multiple metal oxides, synthesized $CoCu_2O_3$ exhibits favourable properties towards applications in solar, thermal and catalytic processes. This progressive contribution applies DFT+U and atomistic thermodynamic approaches to examine the structure and relative stability of $CoCu_2O_3$ surfaces. Twenty-five surfaces along the [001], [010], [100], [011], [101], [110] and [111] low-Miller-indices, with varying surface-termination configurations were selected in this study. The results portray satisfactory geometrical parameters for bulk $CoCu_2O_3$, and a band gap of 1.25 e V. Furthermore, we clarified the stoichiometrically balanced inverted (010)CoCuO, and the non-stoichiometric (001)CuOCu, (001)CoOCo, (110)OCoO and (110)CoOCu surface terminations as the most stable configurations, out of which, the (001)CuOCu shows the optimum stability in ambient conditions. The systematic approach applied in this study should prove instrumental for the analysis of other 3-element multicomponent systems. To the best of our knowledge, the present study is the first to report DFT + U analysis to any 3-multicompnent systems with two of them requires inclusion of U treatment (i.e., *f*- and *d*- orbitals) in the electronic structure calculations.

Keywords: DFT + U; 3-element multicomponent systems; Band gap; Thermodynamic stability

1. Introduction

Critical selection of a stable crystal plane can help improve the reactivity, as well as chemical selectivity of a material. Clearly, this depends on the surface structure and composition, *i.e.*, the arrangements of surface atoms and bonding characteristics of the exposed crystal planes.[1-4] Moreover, in the interest of understanding the function of surfaces under realistic conditions, it is crucial to take into account the influence of surrounding parameters such as the temperature, pressure and the abundance of constituent components in the immediate environment.[5]

Ternary compounds provide richer properties than binary compounds, but also require more complex investigations. Many computational studies for ternary compounds have been conducted, *e.g.* $MgAl_2O_4$ [6], $ZnSnN_2$ [7], CoO-CuO system [8], spinel $LiMn_2O_4$ [9]. Most of these studies express two reservoirs (represented by chemical potentials), while the third reservoir is implied. In this study, we develop rather generally a systematic approach for ternary compounds, which can include transition metal elements, expressed in three reservoirs explicitly. As widely known, transition metals computations require additional approximation to account for strong local electron correlations in its *d*- orbitals. The underlying aim of this study checks the attribute of the aforementioned parameters on the thermodynamic stability of various $CoCu_2O_3$ surface configurations, as a case study.

Cobalt-copper oxides ($Co_xCu_yO_z$) have found distinctive applications in various industrial, such as optical devices, energy conversion and environmental processes. The metal oxides drive the catalysis of the Fischer-Tropsch process, oxygen evolution reactions (EOR), selective oxidation reactions, synthesis of syngas-based alcohol, and similarly serve as potent thermoelectric and high-capacitive electrochemical material.[10-24] Transitional metal oxides also mediate formation of notorious environmental pollutants from their corresponding precursors [25-28]. Synthesised $CoCu_2O_3$ thin film displays favourable solar selectivity and mechanical hardness befitting solar thermal purposes [29; 30]. However, in order to optimize the performance of $CoCu_2O_3$, the knowledge of its stability and local morphology as exposed to different environmental conditions remains important.

Regarding individual cobalt and copper oxides, Zasada et al. reported in their theoretical study that, the (100), (110) and (111) surfaces remain the most stable in Co_3O_4 spinel, while predicting the equilibrium rhombicuboctahedral shape of the nanocrystals [27] under different hydration conditions [31]. Likewise, Soon et al.'s [32] work revealed three surfaces, along the [110] and [111] directions, to have notably lower surface free energies within the allowable range of chemical potentials. The authors reported the catalytic relevancy of Cu_2O(110) terminated with both Cu and O surface atoms, and the Cu_2O(111) containing a coordinative unsaturated Cu vacancy as the energetically-favourable most stable surfaces under oxygen-rich and oxygen-lean conditions[32; 33]. Clean CoO(100) and hydroxylated CoO(111) have also been shown as the most stable Cobalt (II) oxide surface configurations under ethanol steam reforming (ESR) reaction conditions [34].

Furthermore, the mixed metal oxide of Co-Cu-O system exhibits only one major ternary phase, *i.e.*, $CoCu_2O_3$, with CuO, Cu_2O, CoO and Co_3O_4 in binary terminal phases. $CoCu_2O_3$ represents an example of a spin ladder compound by having ~~a~~ high transition temperature superconducting properties. Experimental phrase diagram studies characterized $CoCu_2O_3$ as high-temperature phase that decays into binary oxides approximately below 1180 K, at different oxygen pressures [8; 35]. However directional solidification of the melted phase can result in a considerable amount of $CoCu_2O_3$ at ambient conditions, depending on the fractional–component of metal ions (Cu/Co) [35]. For example, Sekar and co-workers successfully synthesized $CoCu_2O_3$ (form Co_3O_4 and CuO) at high temperature, and preserved it for further experimental analyses between 115 – 300 K [36].

In this paper, we apply density functional theory (DFT) to investigate the geometries of low-Miller-index surfaces (001), (010), (100), (011), (101), (110), and (111) of $CoCu_2O_3$ with various surface-terminations. The results of DFT calculations, performed at T = 0 K and p = 0 atm, have been extrapolated to finite practical temperatures and pressures according to *ab initio* atomistic thermodynamic methodology for multicomponent $CoCu_2O_3$ system. This enables the determination of thermodynamic stability of respective surfaces. Accordingly, we derive propelling conclusions concerning the optimized usage of the ternary-phase metal oxide film in solar and thermal applications.

2. Methodology

2.1. Structural optimisation of bulk and surfaces

VASP package[37] facilitates all structural optimisations and energy calculations for each surface-representative slabs, bulk geometries as well as molecular conformations within the scope of plane wave DFT. The computation details involve the spin-polarized PAW-GGA functional [38], Grimme's van der Waals dispersion correction [39], and Gaussian smearing of 0.2 eV. In plotting projected density of states (PDOS) of the bulk; we deployed the Vosko-Wilk-Nursair interpolation method [40], and a 0.150 peak width of the Gaussian (σ) to broaden the eigenvalues at an electronic temperature of 0.075 eV. Generally, the PDOS of a molecular orbital *m*, ($\rho_m(\varepsilon)$), is computed based on:

$$\rho_m(\varepsilon) = \sum_n \left\langle \phi_m^{MO} \middle| \phi_r \right\rangle \delta(\varepsilon - \varepsilon_n)$$

in which *n* runs over all the states with molecular wavefunctions ϕ_m^{MO} and energy levels ε.

We simulate various $CoCu_2O_3$ surfaces in multi-layer symmetric slab with 30 Å vacuum region separating the periodic images. For Co and Cu systems, it is necessary to apply on-site Coulomb interaction correction (DFT+U) as it enables more accurate band gap estimation. As such, we apply the Dudarev *et al.*'s DFT+U, which has been previously proven to accurately reproduce experimental measurements [41]. We verify our methodology DFT + U methodology for ternary metal oxides by considering a $TiFeO_3$ as literature provides its experimentally measured band gap. The experimental results are provided by Thimsen et al [42]. *J*-value (the on-site exchange parameter) is fixed at 0.95 eV. In the DFT + U treatment, only the difference between *U* and *J* parameters (effective *U*, U_{eff} $=U-J$) parameter accounts for the Coulomb interaction, rendering the choice of the J value to be arbitrary. Nonetheless, our choice for the *J* value follows the commonly deployed value for transitional metals [43]. The results are shown in Fig. 1. The selected *U*-value for TiO_2 and Fe_2O_3 are 13 eVand 8 eV. While for the $TiFeO_3$, we did not perform 3D band gap

landscape calculations, instead U_{Ti} and U_{Fe} of 8 eV is selected to match with the experimental band gap of 2.1 eV.

Fig 1.

Furthermore, the magnetic moments of Co and Cu have also been considered by varying their initial orientations (*i.e.*, ±3.0 for each Co and ±1.0 for each Cu), to obtain the lowest energy. All calculations uses plane wave cut off energy of 500 eV and tight Monkhorst-pack grids [44] serve to perform the Brillouin zone integration. The tolerance on the convergence of the total energy and atomic force equals 10^{-4} eV and 0.05 eV $Å^{-1}$, respectively.

2.2 Thermodynamic stabilities

We employ the results of DFT calculations described above to construct the thermodynamic stability phase diagram comprising all $CoCu_2O_3$ configurations based on the approach of *ab initio* atomistic thermodynamics. The literature describes the physical illustrations and derivations of this formalism [5; 32; 45; 46]. For multi-component systems existing at equilibrium with atomic reservoirs, the most stable surface minimizes the free energy at constant temperature T and pressure p, as defined by:

$$\gamma(T,p) = \frac{1}{A}\left[G^{\text{surf}} - \sum_i N_i \mu_i(T,p)\right] \tag{1}$$

where A, G^{surf}, N, and μ represent the surface area, the Gibbs surface free energy, the number of component atoms, and their atomic chemical potentials, respectively. For symmetric Co-Cu-O system, Equation 1 becomes:

$$\gamma(T,p) = \frac{1}{2A}\left[G^{\text{surf}}(T,p,N_{Co}N_{Cu},N_O) - N_{Co}\mu_{Co}(T,p) - N_{Cu}\mu_{Cu}(T,p) - N_O\mu_O(T,p)\right] \tag{2}$$

Because the surface exists at equilibrium with the underlying bulk oxide, the chemical potentials (μ_{Co}, μ_{Cu} and μ_O) thermodynamically interrelates to one another via the Gibbs free energy of the bulk oxide per unit formula according to Equation 3. Furthermore, the individual chemical potentials can be expressed in terms of relative change on chemical potential $\Delta\mu_i$ and the energy of isolated component energies E_i, as in Equation 4, 5, and 6. E_{Co}^{bulk} and E_{Cu}^{bulk} are energy per unit atom of bulk Co (hexagonal P63/mmc) and Cu (cubic Fm-3m) crystals, while E_{O_2} represents the energy of molecular oxygen.

$$\mu_{Co} + 2\mu_{Cu} + 3\mu_O = g^{bulk}_{CoCu_2O_3}(T,p) \tag{3}$$

$$\mu_{Co}\,(T,p) = \Delta\mu_{Co}(T,p) + E_{Co} \tag{4}$$

$$\mu_{Cu}\,(T,p) = \Delta\mu_{Cu}(T,p) + E_{Cu} \tag{5}$$

$$\mu_O\,(T,p) = \Delta\mu_O(T,p) + \frac{1}{2}E_{O_2} \tag{6}$$

In equation 3, $g^{buk}_{CoCu_2O_3}(T,P)$ signifies Gibbs free energy of the bulk oxide per unit formula. Previous studies [47; 48] have shown that, the Gibbs free energy term can be approximated by the calculated DFT total energy of a specific bulk and/or surface at 0 K and 0 atm:

$$G = E_{DFT} \tag{7}$$

Finally, substitution of Equation 3, 4, 5, 6, and 7 in Equation 2 yields the following governing equations of the *ab initio* atomistic thermodynamics, for determining of surface free energy of a multi-component $CoCu_2O_3$ system existing at equilibrium with the atomic reservoir of the surrounding oxygen gas and the macroscopic bulk of copper or cobalt:

$$\begin{aligned}\gamma(\Delta\mu_{Cu,}\Delta\mu_O) &= \frac{1}{2A}\Big[E^{surf} - N_{Co}E^{bulk}_{CoCu_2O_3} - (N_{Cu} - 2N_{Co})\big(E^{bulk}_{Cu} + \Delta\mu_{Cu}\big) \\ &\quad - (N_O - 3N_{Co})\left(\tfrac{1}{2}E_{O_2} + \Delta\mu_O\right)\Big]\end{aligned} \tag{8}$$

$$\gamma(\Delta\mu_{Co,}\Delta\mu_O) = \frac{1}{2A}\Big[E^{surf} - \tfrac{1}{2}N_{Cu}E^{bulk}_{CoCu_2O_3} - \Big(N_{Co} - \tfrac{1}{2}N_{Cu}\Big)\big(E^{bulk}_{Co} + \Delta\mu_{Co}\big) - \Big(N_O - \tfrac{3}{2}N_{Cu}\Big)\Big(\tfrac{1}{2}E_{O_2} + \Delta\mu_O\Big)\Big] \quad (9)$$

It must be noted that in Equation of 8 and 9, the $\gamma(T,p)$ dependencies are imposed only by $\Delta\mu_{Co}\,(T,p)$, $\Delta\mu_{Cu}\,(T,p)$ and $\Delta\mu_O\,(T,p)$. However, the variations in chemical potentials have feasible allowable range. For instance, $\Delta\mu_O\,(T,p)$ is bounded by oxygen-lean conditions (denoting the commencement of the formation of a $CoCu_2O_3$ bulk upon the presence of cobalt and copper bulks in a phase reservoir of oxygen gas; relatively, this also implies the condition where the $CoCu_2O_3$ bulk tends to decompose into constituent metal/metal oxides and oxygen gas), and oxygen-rich limit (signifying the condensation of O_2 gas on the surface). The oxygen-lean limit is arbitrary considered to be the enthalpy of the formation of the metal oxide [45; 49]. Similarly, Cu and/or Co can be abundant or deficient depending on the surrounding macroscopic composition of the respective bulk as well as individual bulk oxides. The reasonable estimates for $\Delta\mu_i$ limits at equilibrium are given by the following simultaneous inequalities.

$$\mathrm{Max}(\Delta\mu_{Co}) = \mathrm{Max}(\Delta\mu_{Cu}) = \mathrm{Max}(\Delta\mu_O) = 0; \quad (10)$$

$$\mathrm{Min}\big(\Delta\mu_{Cu} + \tfrac{3}{2}\Delta\mu_O\big) = \frac{E^{\mathrm{bulk}}_{CoCu_2O_3} - E^{\mathrm{bulk}}_{Co}}{2} - E^{\mathrm{bulk}}_{Cu} - \tfrac{3}{4}E^{\mathrm{gas}}_{O_2} \quad \text{For eqn (8)} \quad (11)$$

$$\mathrm{Min}(\Delta\mu_{Co} + 3\Delta\mu_O) = E^{\mathrm{bulk}}_{Cu_2CoO_3} - 2E^{\mathrm{bulk}}_{Cu} - E^{\mathrm{bulk}}_{Co} - \tfrac{3}{2}E^{\mathrm{gas}}_{O_2} \quad \text{For eqn (9)} \quad (12)$$

Furthermore, we estimate the temperature and pressure dependencies of $\Delta\mu_i$ from the values presented in NIST-JANAF thermodynamics table,[50] according to:

$$\Delta\mu_{Cu}(T,p) = [H_{Cu}(T,p^\circ) - H_{Cu}(T^\circ,p^\circ)] - T[S_{Cu}(T,p^\circ) - S_{Cu}(T^\circ,p^\circ)] + kTln\frac{p}{p^\circ} \quad (13)$$

$$\Delta\mu_{Co}(T,p) = [H_{Co}(T,p^\circ) - H_{Co}(T^\circ,p^\circ)] - T[S_{Co}(T,p^\circ) - S_{Co}(T^\circ,p^\circ)] + kTln\frac{p}{p^\circ} \quad (14)$$

$$\Delta\mu_O(T,p) = \tfrac{1}{2}\big[H_{O_2}(T,p^\circ) - H_{O_2}(T^\circ,p^\circ)\big] - \tfrac{T}{2}\big[S_{O_2}(T,p^\circ) - S_{O_2}(T^\circ,p^\circ)\big] + \tfrac{1}{2}kTln\frac{p}{p^\circ} \quad (15)$$

where H, S, T°, p° denote NIST-JANAF's enthalpy, entropy, reference temperature (0 K), reference pressure (100 kPa) of the reservoirs; and T, p, k are temperature, pressure, Boltzmann constant (8.617×10^{-5} eV/K), respectively.

3. Results and discussion

3.1. Crystallographic structural parameter of bulk $CoCu_2O_3$

The adopted DFT+U method requires us to obtain suitable U-J parameters. For bulk $CoCu_2O_3$, we fixed the J-value at 0.95 eV, and selected the best U-value of 9.5 eV (Fig. 1). This U-value was selected based on the following simultaneous conditions: (a) the proximity to the U-value range of cubic CoO and monoclinic CuO (see Fig. 2), and (b) the band gap presence in the $CoCu_2O_3$. The bulk calculation uses 4 × 8 × 10 k-point of Monkhorst-Pack scheme and gamma-centred grid for geometric optimisation, as well as 8 × 16 × 20 k-point for reliable computation of density of states (DOS). In addition, we investigated the contribution of the magnetic moment initial orientations for each Co and Cu atoms, and the optimum directions, in terms of lowest bulk energy, are presented in Fig. 3. The final magnitudes of the vectors were obtained *via* self-consistent calculations. This reveals the ferromagnetism of bulk $CoCu_2O_3$, besides its semiconducting nature.

Combining these U-value and magnetic moment orientations gives the lowest bulk energy and also a band gap of 1.25 eV. Figure 4 plots the band structure (a) and PDOS (b) for bulk $CoCu_2O_3$. To the best of our knowledge, there is no experimental data for the band gap of $CoCu_2O_3$. Bulk $CoCu_2O_3$ exhibits orthorhombic crystal structure with *Pmmn* space group, and our calculated lattice constants; a = 9.45 Å, b = 3.96 Å and c = 3.19 Å agree well with the corresponding experimental values 9.41 Å, 3.98 Å and 3.20 Å (from XRD database ICDD 76-0442). Inspecting further the PDOS of bulk $CoCu_2O_3$ in Fig. 4b, it is seen that oxygen dominates the valence band near the Fermi energy, copper dominates the conduction band near the Fermi energy, while cobalt dominates the higher band beyond the conduction band.

Fig. 2

Fig. 3

Fig. 4

3.2. Geometries of low-Miller-index $CoCu_2O_3$ surfaces

Having obtained accurate results for bulk $CoCu_2O_3$, we consider all low-Miller-index orientations of $CoCu_2O_3$ surfaces, namely, (001), (010), (100), (011), (101), (110) and (111) with various plausible terminations. Each slab has been relaxed with 15 Å vacuum distances at both symmetric ends, and we reused the *U*-value and magnetic moment orientations of the bulk structure. We also impose magnetic moment pair for Cu, and consider the surfaces with atomic ratio, *i.e.*, Co:Cu:O nearing 1:2:3. Refer to Table S1 in the Supplementary Information for further details on the 25 slabs thicknesses and *k*-points used in the calculations. Fig. 5portrays the optimized minimum energy structure of 25 surfaces, and Table 1 lists their prominent characteristics

Fig. 5

Table 1

Subsequent discussions refer to the surfaces based on their planar orientations and elemental terminations. For example, the (001)CuOCo surface represents a construction truncated along the [001] direction with Cu/O/Co atoms located in the outmost layer, in sequential order. As seen in Table 1, ten different surfaces exist in the stoichiometry state of $CoCu_2O_3$, *i.e.*, atomic ratio Co:Cu:O = 1:2:3. Meanwhile, the non-stoichiometric surfaces have also been listed with their respective atomic deficiencies with respect to cobalt and copper.

3.3. Thermodynamic stability phase diagram

Equation 10, 11, and 12 afford the estimation of a physical allowable range of change in chemical potentials as follows:

$-9.48 < \Delta\mu_{Co} < 0\ eV$,

$-4.74 < \Delta\mu_{Cu} < 0\ eV$, and

$-3.16 < \Delta\mu_{O} < 0\ eV$.

Furthermore the distribution of $\Delta\mu(T,p)$ within the specified limits from Equation 13, 14 and 15 were computed. Fig. 6 depicts the calculated change in chemical potential over a temperature range of 0 K to 2000 K, and pressures between ultra-high vacuum (100 nPa) to high-pressure regime (10 GPa).

Fig. 6

Cobalt incurs the widest range for change in chemical potential. In fact, as seen in Fig. 6, it is clear that over the selected surrounding temperature and pressure conditions, $\Delta\mu_{Co}(T,p)$ exceeds its minimum value, *i.e.*, its Co-lean limit. Hence from a physical viewpoint, it may be more noteworthy to preferentially consider Equation 8 for the calculation of surface free energy. However, Equation 9 leads also to the same computational deductions. The explicit forms of $\gamma(\Delta\mu_{Cu,}\Delta\mu_{O})$ and $\gamma(\Delta\mu_{Co,}\Delta\mu_{O})$ are presented in Table S4 in the Supplementary Information.

Table 2 presents the calculated surface free energy of all stoichiometric surfaces (see Fig. S1 in the Supplementary Information for the 3-D plot). As expected, all the surface configurations with Co:Cu:O = 1:2:3 exhibit a constant free energy value (seen as flat planes in Fig. 6), and the minimum $\gamma(T,p)$ lies on the inverted (010)CoCuO termination.

Table 2

Thereafter, we compare the non-stoichiometric surfaces with (010)$CoCuO_{inv}$ (see Fig. S2 in the Supplementary Information for the 3-D plot). Fig. 6 depicts the two-dimensional contour plane of the section. Over the considered change in chemical potential ranges, some non-stoichiometric surface appear more stable than (010)$CoCuO_{inv}$. The scale of $\Delta\mu_{Co}$ and $\Delta\mu_{Cu}$ in Fig. 7 indicates that, the facet characteristics at the lean Cu is qualitatively similar to rich Co and *vice versa*. Notably, at the lean Cu/rich Co/rich O, the surface energies of

(001)CoOCo and (110)OCoO are lower than that in bulk, indicating that these surfaces form spontaneously at such conditions.

Fig. 7

Applicably, one can easily calculate the $\Delta\mu_{Cu}$ and $\Delta\mu_O$ values corresponding to a particular temperature and pressure from Equation 13, 14, 15 (or by inspection of Fig. 6), an then trace out the most stable surface configuration for the intended conditions. For example, at ambient environmental conditions (T = 298.15 K, and p = 1 atm), the $\Delta\mu_{Cu}$ and $\Delta\mu_O$ respectively equal to –0.05 eV and –0.27 eV, hence the (001)CuOCu represents the optimum surface configuration for such applications. Refer to Fig. S3 (Supplementary Information) for further examples.

In addition, we tuned the $\Delta\mu_O$ parameters at constant $\Delta\mu_{Cu}$ values. Theoretically, the surface free energy of a stoichiometric surface composition remains independent of the gas phase chemical potential, and conversely, a surface termination with excess oxygen will become more stable while those with an oxygen deficiency will be less stable with increasing gas phase chemical potential [45; 49].

Fig. 8

The trends in Fig. 8 illustrates that, (001)CuOCu surface termination incur surplus oxygen, whereas, the other slabs are relatively O deficient over the considered gas-phase chemical potentials. Consequently, (001)CuOCu becomes more stable with increase in $\Delta\mu_O$. Furthermore, this is justified by referring to Table 1, (001)CuOCu has relatively large Cu/O excess (4, 4) with respect to Co. However, the situation is contrary for (110)OCoO, (001)CoOCo, (110)CoOCu surfaces, having O deficit of –2, –4, and –6, in that order with respect to Co. Our findings herein is consistent with the general consensus that non-stoichiometric surfaces with surplus of electro negatively charged atoms (such as O and halides)[47-49] tend to be more thermodynamically stable. In our recent study on thermodynamic stability of $CuBr_2$ surfaces [48], we illustrated that many structural and electronic factors may contribute to the stability ordering such as the degree of surface relaxation, reduction in the charge in the topmost layer as well as the overall polarity of the

slab. Herein, the profound stability of the (001)CuOCu most likely stems from the surface polarity induced by its non-stoichiometric termination.

4. Conclusions

The structures and surface stabilities of transition metallic (oxide) ternary compounds have been studied *via* accurate DFT+U method amalgamated with *ab initio* atomistic thermodynamics. As a case study, we examined the $CoCu_2O_3$ surfaces with regards to bulk Co/Cu and O_2 gas reservoirs, and presented the suitable stability phase diagram. The chemical potential range of the componential species represents the key variable in the atomistic thermodynamics. Within the considered range for change in chemical potentials, our result elucidated five stable surfaces across all low-Miller-index directions. This includes the stoichiometrically balanced (010)$CoCuO_{inv}$, and the non-stoichiometric (001)CuOCu, (001)CoOCo, (110)OCoO and (110)CoOCu facet terminations. Considerably, (001)CuOCu represents the optimum surface configuration for applications in ambient conditions. Furthermore, the (001)CoOCo and (110)OCoO surface configurations can be formed spontaneously at certain rare conditions. Finally, the systematic approach applied in this study can be easily employed for the analysis: (1) of other 3-element multicomponent systems (including transition metal elements); (2) on the higher Miller-index surfaces; and (3) of surface phase transition as a function of reservoirs, temperature and pressure. Accordingly, we derive propelling conclusions concerning the optimized usage of the ternary-phase metal oxide film in solar and thermal applications.

Acknowledgements

This study has been supported by the Innovative Research Universities – Malaysian Research University Network (IRU-MRUN) Collaborative Research Programme, as well as grants of computing time from the National Computational Infrastructure (NCI) in Canberra and from the Pawsey Supercomputing Centre in Perth, Australia.

Supporting Information: Tables S1-S3, Figures S1-S3.

References

[1] X. Xie, Y. Li, Z.-Q. Liu, M. Haruta, W. Shen, Low-temperature oxidation of CO catalysed by Co_3O_4 nanorods, Nature 458 (2009) 746-749.

[2] X. Liu, K. Zhou, L. Wang, B. Wang, Y. Li, Oxygen vacancy clusters promoting reducibility and activity of ceria nanorods, J. Amer. Che. Soc. 131 (2009) 3140-3141.

[3] T. Xie, M. Gong, Z. Niu, S. Li, X. Yan, Y. Li, Shape-controlled CuCl crystallite catalysts for aniline coupling, Nano Res. 3 (2010) 174-179.

[4] Y. Kwon, A. Soon, H. Han, H. Lee, Shape effects of cuprous oxide particles on stability in water and photocatalytic water splitting, J. Mater. Chem: A 3 (2015) 156-162.

[5] C. Stampfl, Surface processes and phase transitions from ab initio atomistic thermodynamics and statistical mechanics, Catal. Today 105 (2005) 17-35.

[6] X. Li, Q. Hui, D.-Y. Shao, J.-J. Chen, C.-M. Li, N.-P. Cheng, Stability and electronic structure of $MgAl_2O_4$(1 1 1) surfaces: A first-principles study, Comput. Mater. Sci. 112, Part A (2016) 8-17.

[7] S. Chen, P. Narang, H.A. Atwater, L.-W. Wang, Phase Stability and Defect Physics of a Ternary $ZnSnN_2$ Semiconductor: First Principles Insights, Adv. Mater. 26 (2014) 311-315.

[8] L.A. Zabdyr, O.B. Fabrichnaya, Phase equilibria in the cobalt oxide-copper oxide system, J. Phase. Equilib. 23 (2002) 149-155.

[9] R.E. Warburton, H. Iddir, L.A. Curtiss, J. Greeley, Thermodynamic stability of low- and high-Index spinel LiMn2O4 surface terminations, ACS Appl. Mater. Interfaces 8 (2016) 11108-11121.

[10] D.J. Singh, Electronic and thermoelectric properties of $CuCoO_2$: Density functional calculations, Phys. Rev. B 76 (2007) 085110-085113.

[11] G.G. Volkova, T.A. Krieger, L.M. Plyasova, V.A. Zaikovskii, T.M. Yurieva, Copper-cobalt catalysts for higher alcohols synthesis from syngas, 1997, 67-72.

[12] G.G. Volkova, T.M. Yurieva, L.M. Plyasova, M.I. Naumova, V.I. Zaikovskii, Role of the Cu-Co alloy and cobalt carbide in higher alcohol synthesis, J. Mol. Catal. Chem. 158 (2000) 389-393.

[13] G. Fornasari, S. Gusi, F. Trifiro, A. Vaccari, Cobalt mixed spinels as catalysts for the synthesis of hydrocarbons, Indust. Eng. Chem. Res. 26 (1987) 1500-1505.

[14] M. De Koninck, S.-C. Poirier, B. Marsan, $Cu_xCo_{3-x}O_4$ Used as bifunctional electrocatalyst physicochemical properties and electrochemical characterization for the oxygen evolution reaction, J. Elecrochem. Soc. 153 (2006) A2103-A2110.

[15] M. Beekman, J. Salvador, X. Shi, G.S. Nolas, J. Yang, Characterization of delafossite-type $CuCoO_2$ prepared by ion exchange, J. Alloy. Compd. 489 (2010) 336-338.

[16] B. Marsan, N. Fradette, G. Beaudoin, Physicochemical and Electrochemical Properties of CuCo2 O 4 Electrodes Prepared by Thermal Decomposition for Oxygen Evolution, J. Elecrochem. Soc. 139 (1992) 1889-1896.

[17] J.L. Gautier, E. Trollund, E. Ríos, P. Nkeng, G. Poillerat, Characterization of thin $CuCo_2O_4$ films prepared by chemical spray pyrolysis. Study of their electrochemical stability by ex situ spectroscopic analysis, J. Electroanal. Chem. 428 (1997) 47-56.

[18] R. Bonchev, T. Zheleva, S.C. Sevov, Morphological and compositional characterization of copper-cobalt spinel made by mechanochemical reactions, Chem. Mater. 2 (1990) 93-95.

[19] S. Angelov, D. Mehandjiev, B. Piperov, V. Zarkov, A. Terlecki-Baričević, D. Jovanović, Ž. Jovanović, Carbon monoxide oxidation on mixed spinels CuxCo3-xO4 in the presence of sulphur compounds, Appl. Catal. 16 (1985) 431-437.
[20] X. Xiaoding, E.B.M. Doesburg, J.J.F. Scholten, Synthesis of higher alcohols from syngas - recently patented catalysts and tentative ideas on the mechanism, Catal. Today 2 (1987) 125-170.
[21] J.E. Baker, R. Burch, S.E. Golunski, Synthesis of higher alcohols over copper/cobalt catalysts. Influence of preparative procedures on the activity and selectivity of Cu/Co/Zn/Al mixed oxide catalysts, Appl. Catal. 53 (1989) 279-297.
[22] K. Fujimoto, T. Oba, Synthesis of C_1-C_7 alcohols from synthesis gas with supported cobalt catalysts, Appl. Catal. 13 (1985) 289-293.
[23] Z.Y. Tian, H. Vieker, P.M. Kouotou, A. Beyer, In situ characterization of Cu-Co oxides for catalytic application, Farad. Discuss. 177 (2015) 249-262.
[24] A. Shanmugavani, R.K. Selvan, Improved electrochemical performances of CuCo2O4/CuO nanocomposites for asymmetric supercapacitors, Electrochimica Acta 188 (2016) 852-862.
[25] M. Altarawneh, B.Z. Dlugogorski, Formation of dibenzofuran, dibenzo-*p*-dioxin and their hydroxylated derivatives from catechol, Phys. Chem. Chem. Phys. 17 (2015) 1822-1830.
[26] M. Altarawneh, M.W. Radny, P.V. Smith, J.C. Mackie, E.M. Kennedy, B.Z. Dlugogorski, A. Soon, C. Stampfl, A first-principles density functional study of chlorophenol adsorption on Cu_2O(110):CuO, J. Chem. Phys. 130 (2009) 184505-184512.
[27] M. Altarawneh, B.Z. Dlugogorski, Mechanism of Thermal Decomposition of Tetrabromobisphenol A (TBBA), J. Phys. Chem. A. 118 (2014) 9338-9346.
[28] M. Altarawneh, B.Z. Dlugogorski, Formation and Chlorination of Carbazole, Phenoxazine, and Phenazine, Environ. Sci. Technol. 49 (2015) 2215-2221.
[29] A. Amri, X. Duan, C.-Y. Yin, Z.-T. Jiang, M.M. Rahman, T. Pryor, Solar absorptance of copper–cobalt oxide thin film coatings with nano-size, grain-like morphology: Optimization and synchrotron radiation XPS studies, Appl. Surf. Sci. 275 (2013) 127-135.
[30] A. Amri, Z.-T. Jiang, P.A. Bahri, C.-Y. Yin, X. Zhao, Z. Xie, X. Duan, H. Widjaja, M.M. Rahman, T. Pryor, Surface Electronic Structure and Mechanical Characteristics of Copper–Cobalt Oxide Thin Film Coatings: Soft X-ray Synchrotron Radiation Spectroscopic Analyses and Modeling, J. Phys. Chem. C. 117 (2013) 16457-16467.
[31] F. Zasada, W. Piskorz, S. Cristol, J.-F. Paul, A. Kotarba, Z. Sojka, Periodic density functional theory and atomistic thermodynamic studies of cobalt Spinel Nanocrystals in wet environment: Molecular Interpretation of water adsorption equilibria, J. Phys. Chem. C. 114 (2010) 22245-22253.
[32] A. Soon, M. Todorova, B. Delley, C. Stampfl, Thermodynamic stability and structure of copper oxide surfaces: A first-principles investigation, Phys. Rev. B 75 (2007) 125420-125429.
[33] A. Soon, M. Todorova, B. Delley, C. Stampfl, Erratum: Thermodynamic stability and structure of copper oxide surfaces: A first-principles investigation Phys. Rev. B 76 (2007) 129902-129903.
[34] W. Luo, A. Asthagiri, An ab initio thermodynamics study of cobalt surface phases under ethanol steam reforming conditions, Catal. Sci. Technol. 4 (2014) 3379-3389.
[35] N. Wizent, L. Schramm, G. Behr, W. Löser, W. Gruner, A. Voß, B. Büchner, L. Schultz, Phase diagram features and solidification behaviour of $CoCu_2O_3$ at elevated oxygen pressure, J. Solid State Chem. 182 (2009) 2036-2040.

448 [36] C. Sekar, S. Paulraj, G. Krabbes, M. Kanagaraj, S. Arumugam, R.S. Kumar,
449 Synthesis, structural and magnetic properties of spin ladder compound $Ca_{1-x}CoxCu_2O_3$,
450 J.Magn. Magn. Mater 323 (2011) 3033-3037.
451 [37] G. Kresse, J. Furthmüller, Efficient iterative schemes for ab initio total-energy
452 calculations using a plane-wave basis set, Phys. Rev. B. 54 (1996) 11169-11186.
453 [38] J.P. Perdew, K. Burke, Y. Wang, Generalized gradient approximation for the
454 exchange-correlation hole of a many-electron system, Phys. Rev. B 54 (1996) 16533-16539.
455 [39] S. Grimme, Semiempirical GGA-type density functional constructed with a long-
456 range dispersion correction, J. Comput. Chem. 27 (2006) 1787-1799.
457 [40] S.H. Vosko, L. Wilk, M. Nusair, Accurate spin-dependent electron liquid correlation
458 energies for local spin density calculations: a critical analysis, Can. J. Phys. 58 (1980) 1200-
459 1211.
460 [41] S.L. Dudarev, G.A. Botton, S.Y. Savrasov, C.J. Humphreys, A.P. Sutton, Electron-
461 energy-loss spectra and the structural stability of nickel oxide: An LSDA+U study, Phys.
462 Rev. B 57 (1998) 1505-1509.
463 [42] E. Thimsen, S. Biswas, C.S. Lo, P. Biswas, Predicting the band structure of mixed
464 transition metal oxides: theory and experiment, J. Phys. Chem. C. 113 (2009) 2014-2021.
465 [43] M. Benouis, Y. Azzaz, M. Ameri, O. Arbouche, A. Bennadji, D. Bensaid, Y. Al-
466 Douri, Electronic and magnetic properties of Cr_2GeC with GGA + U approximation, J.
467 Supercond. Nov. Magn. 29 (2016) 1267-1272.
468 [44] H.J. Monkhorst, J.D. Pack, Special points for Brillouin-zone integrations, Phys. Rev.
469 B 13 (1976) 5188-5192.
470 [45] J. Rogal, K. Reuter, M. Scheffler, First-Principles Statistical Mechanics Study of the
471 Stability of a Subnanometer Thin Surface Oxide in Reactive Environments: CO Oxidation at
472 Pd(100), Phys. Rev. Lett. 98 (2007) 046101-046105.
473 [46] R.E. Warburton, H. Iddir, L.A. Curtiss, J. Greeley, Thermodynamic Stability of Low-
474 and High-Index Spinel LiMn2O4 Surface Terminations, ACS applied materials & interfaces
475 8 (2016) 11108-11121.
476 [47] M. Altarawneh, Z.-T. Jiang, B.Z. Dlugogorski, The structures and thermodynamic
477 stability of copper(II) chloride surfaces, Phys. Chem. Chem. Phys. 16 (2014) 24209-24215.
478 [48] M. Altarawneh, A. Marashdeh, B.Z. Dlugogorski, Structures, electronic properties
479 and stability phase diagrams for copper(I/II) bromide surfaces, Phys. Chem. Chem. Phys. 17
480 (2015) 9341-9351.
481 [49] J. Rogal, K. Reuter, M. Scheffler, Thermodynamic stability of PdO surfaces, Phys.
482 Rev. B 69 (2004) 075421-075428.
483 [50] M.W. Chase, S. National Institute of, Technology, NIST-JANAF thermochemical
484 tables, American Chemical Society ; American Institute of Physics for the National Institute
485 of Standards and Technology, [Washington, D.C.]; Woodbury, N.Y., 1998.

486

487

488

Table 1 The geometry $CoCu_2O_3$ surfaces.

No.	Miller-index	Near surface atoms	Slab composition (Co:Cu:O)	Cu, O excess/deficit with respect to Co	Co, O excess/deficit with respect to Cu	Surface area ($Å^2$)
1[a]	001	Cu, O, Co	8:16:24	0, 0	0, 0	37.43
2	001	Co, O, Co	10:16:26	–4, –4	2, 2	37.43
3[a]	001	Co, O, Cu	8:16:24	0, 0	0, 0	37.43
4	001	Cu, O, Cu	6:16:22	4, 4	–2, –2	37.43
5	001	O, Co, O	8:16:26	0, 2	0, 2	37.43
6	001	O, Cu, O	8:16:28	0, 4	0, 4	37.43
7[a]	010	Co, Cu, O (inverted)	8:16:24	0, 0	0, 0	30.19
8[a]	010	Co, Cu, O (mirrored)	9:18:27	0, 0	0, 0	30.19
9[a]	100	Cu, O, Co	3:6:9	0, 0	0, 0	12.66
10	100	Co, O, Cu	5:8:13	–2, –2	1, 1	12.66
11	100	Cu, O, Cu	3:8:11	2, 2	–1, –1	12.66
12[a]	011	Cu, O, Co	10:20:30	0, 0	0, 0	48.09
13[a]	011	Cu, Co, O	10:20:30	0, 0	0, 0	48.09
14[a]	101	Co, Cu, O	10:20:30	0, 0	0, 0	39.51
15	101	O, Cu, O	8:20:30	4, 6	–2, 0	39.51
16	101	Cu, O, Cu	8:20:26	4, 2	–2, –4	39.51
17[a]	101	Cu, Cu, O	8:16:24	0, 0	0, 0	39.51
18	101	Co, O, O	8:12:22	–4, –2	2, 4	39.51
19	110	O, Cu, O	6:16:24	4, 6	–2, 0	32.73
20	110	Cu, O, Cu	6:16:20	4, 2	–2, –4	32.73
21	110	Cu, O, O	6:12:20	0, 2	0, 2	32.73
22	110	Cu, O, Co	6:12:16	0, –2	0, –2	32.73
23	110	O, Co, O	6:8:16	–4, –2	2, 4	32.73
24	110	Co, O, Cu	8:12:18	–4, –6	2, 0	32.73
25[a]	111	Co, Cu, O	10:20:30	0, 0	0, 0	49.73

[a] Surface with atomic ratio of Co:Cu:O = 1:2:3

Table 2 Surface free energies of $CoCu_2O_3$ slabs with atomic ratio of Co:Cu:O = 1:2:3

No.	Miller-index	Near surface atoms	Surface free energy (eV/Å^2)
1	001	Cu, O, Co	0.17
3	001	Co, O, Cu	0.14
7	010	Co, Cu, O (inverted)	0.09
8	010	Co, Cu, O (mirrored)	0.10
9	100	Cu, O, Co	0.18
12	011	Cu, O, Co	0.12
13	011	Cu, Co, O	0.19
14	101	Co, Cu, O	0.11
17	101	Cu, Cu, O	0.12
25	111	Co, Cu, O	0.12

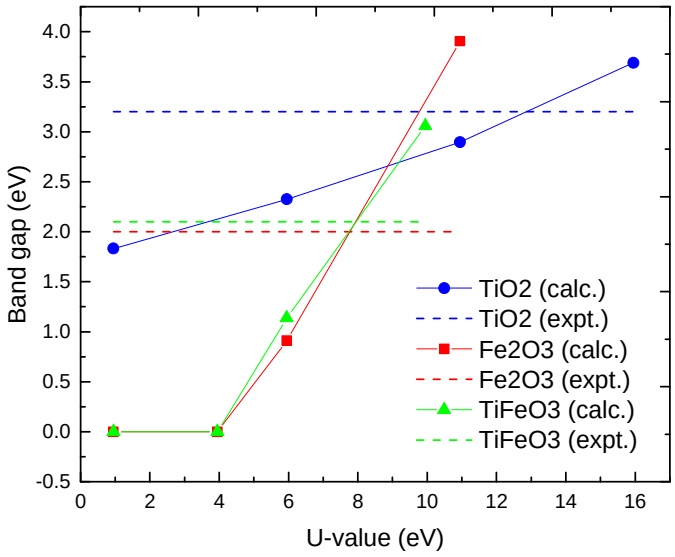

Fig. 1. Band gaps of anatase TiO_2, hematite Fe_2O_3 and ilmenite $TiFeO_3$ with respect to varying *U*-values. Experimental values are sourced from Ref [36].

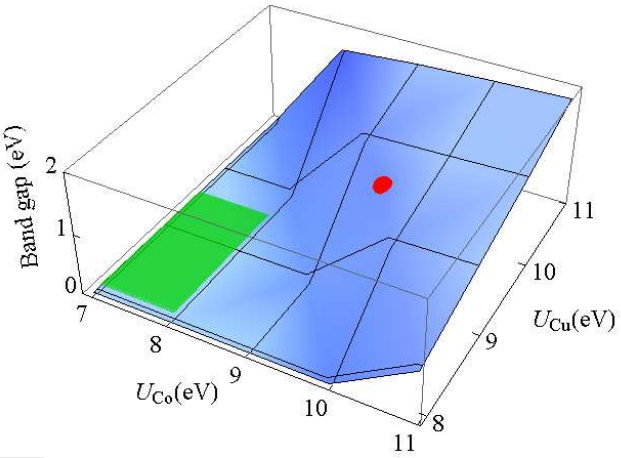

Fig. 2 $CoCu_2O_3$ band gaps with respect to varying U_{Co} and U_{Cu} values. Red dot represents the selected *U*-values. Green surface is the *U*-value range for cubic CoO and monoclinic CuO.

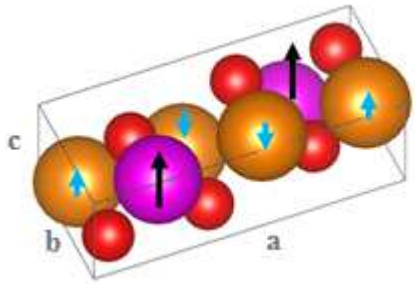

Fig. 3 Magnetic moments of bulk $CoCu_2O_3$. Purple, brown and red spheres represents Co, Cu and O atoms; respectively. The lattice constants a = 9.45 Å, b = 3.96 Å and c = 3.19 Å. Black and blue arrows are the magnetic moment orientations with magnitude of 2.89 μ_B and 0.76 μ_B, respectively.

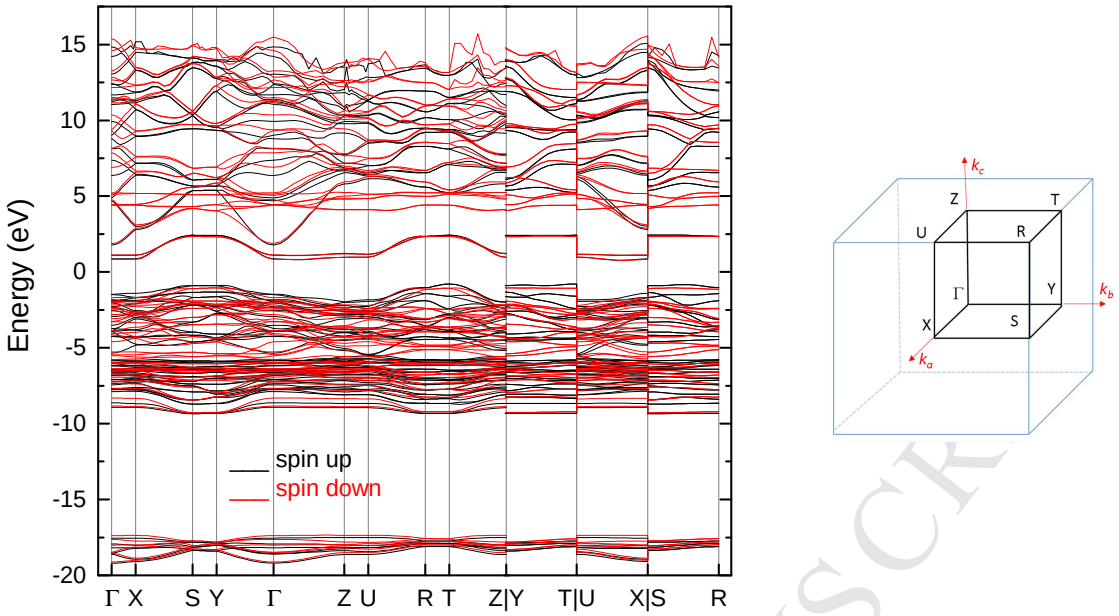

(a)

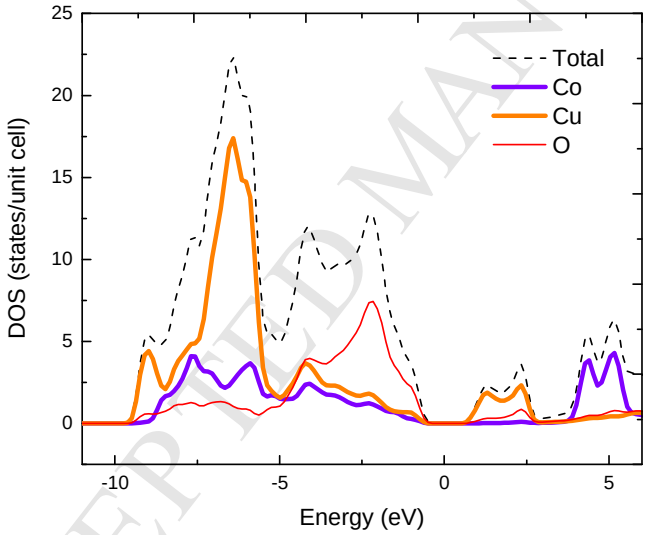

(b)

Fig. 4 (a) Band structure and (b) projected density of states (total spin) of bulk $CoCu_2O_3$. Estimated band gap ≈1.25 eV.

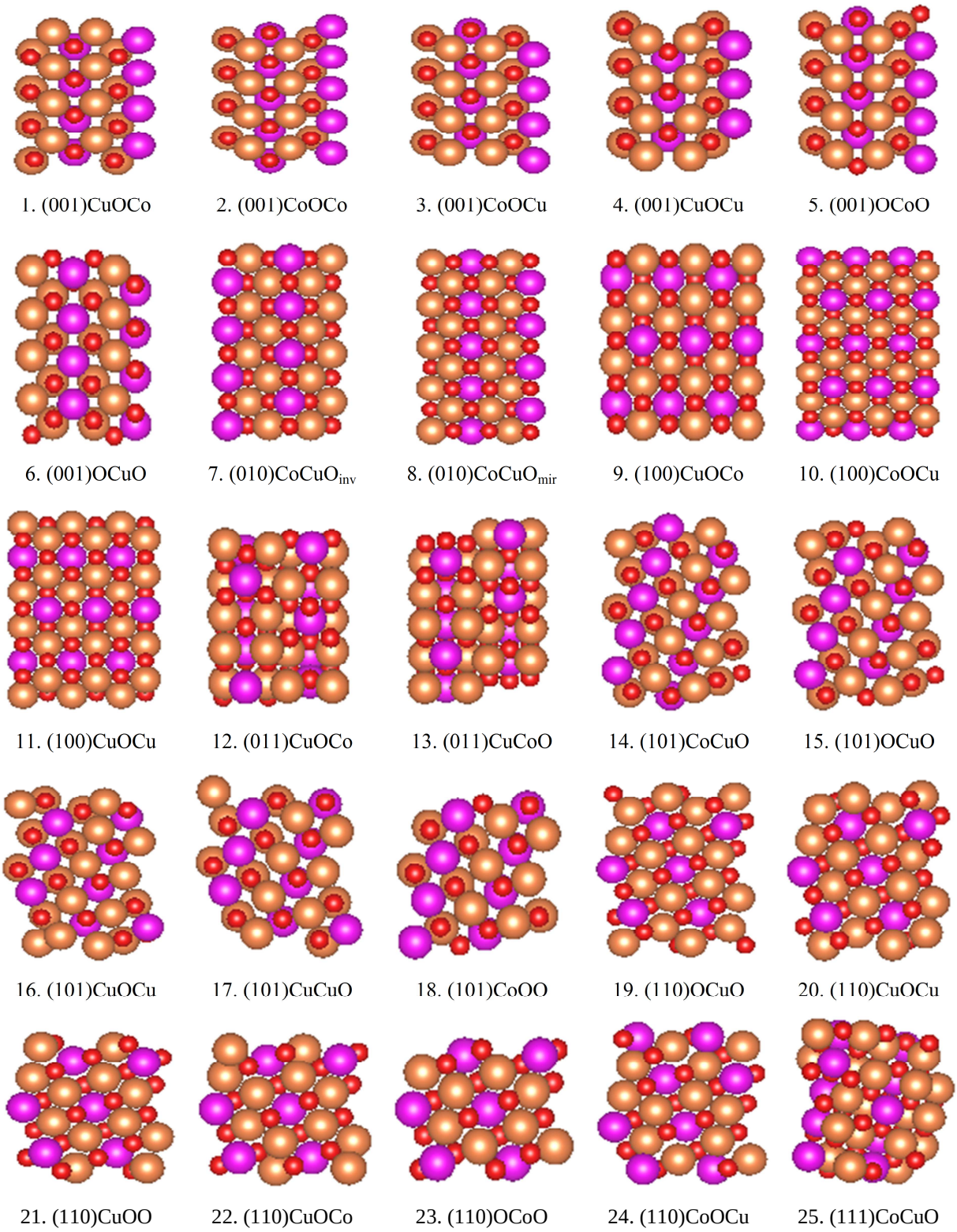

Fig. 5 Vertical cross sections of the optimized $CoCu_2O_3$ surfaces. Purple, brown and red denote Co, Cu and O, respectively.

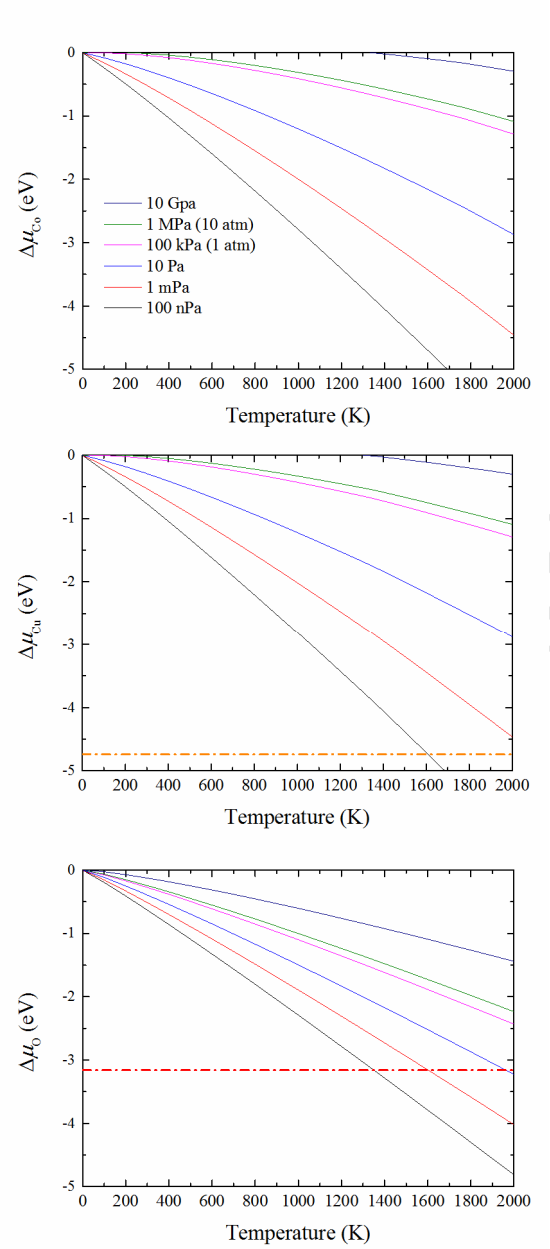

Fig. 6 $\Delta\mu_{Co}(T,p)$, $\Delta\mu_{Cu}(T,p)$ and $\Delta\mu_{O}(T,p)$ as calculated by NIST-JANAF thermodynamics table via Equation 13, 14 and 15. Minimum chemical potential (dashed line) was set according to Equation 10, 11 and 12.

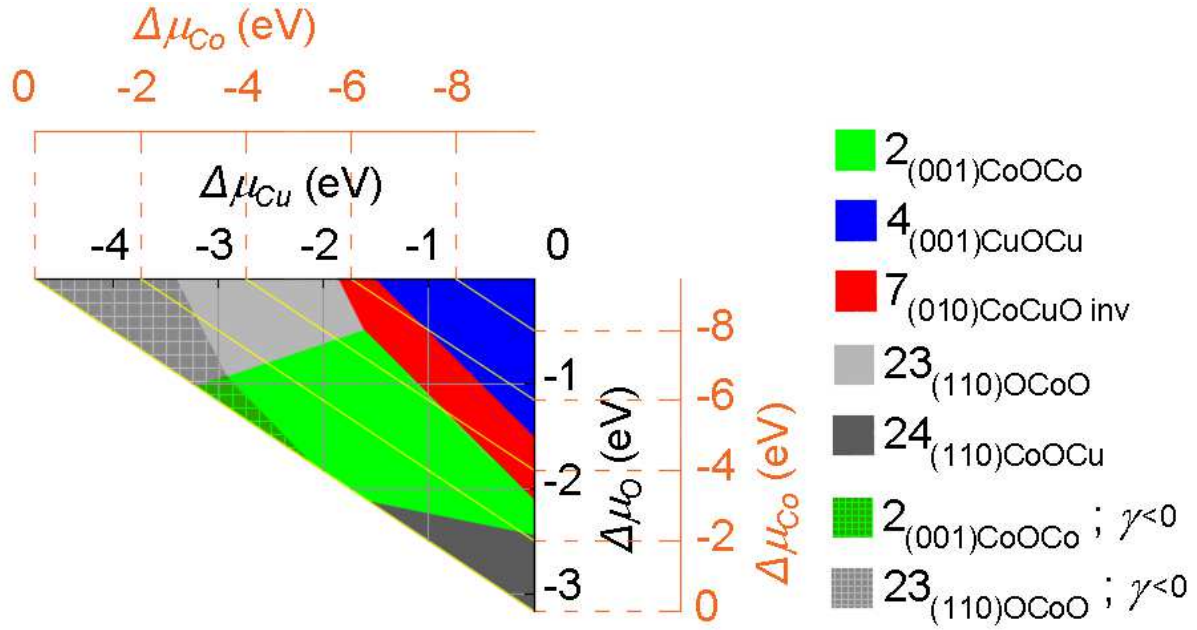

Fig. 7 The most stable phase diagram of $\gamma(\Delta\mu_{Cu,}\Delta\mu_O)$ and $\gamma(\Delta\mu_{Co,}\Delta\mu_O)$ for all inspected surfaces. γ is surface free energy (eV/Å^2) and $\Delta\mu$ is chemical potential variation of the respective atom (eV). Diagonal brown line indicates $\Delta\mu_{Co}$.

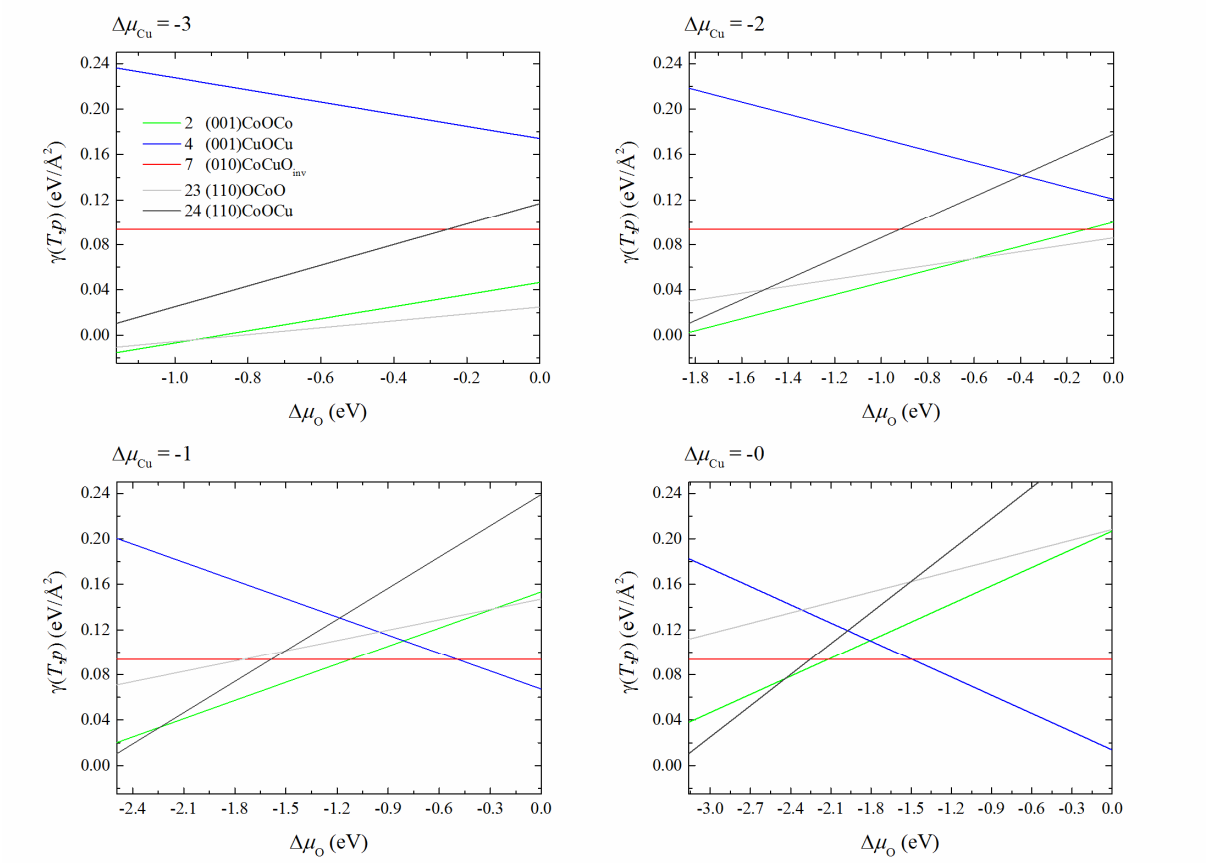

Fig. 8 Surface energies of the most stable surface terminations for low-index surface facets considered in this work. $\Delta\mu_O$ (drawn at different scales) is considered as tuneable parameter under fixed $\Delta\mu_{Cu}$ values. Negative gradient (line sloping downward from left to right) signifies slabs with excess O, and positive gradient (line sloping upward from left to right) represent slabs with O deficiency.

Table of content entry

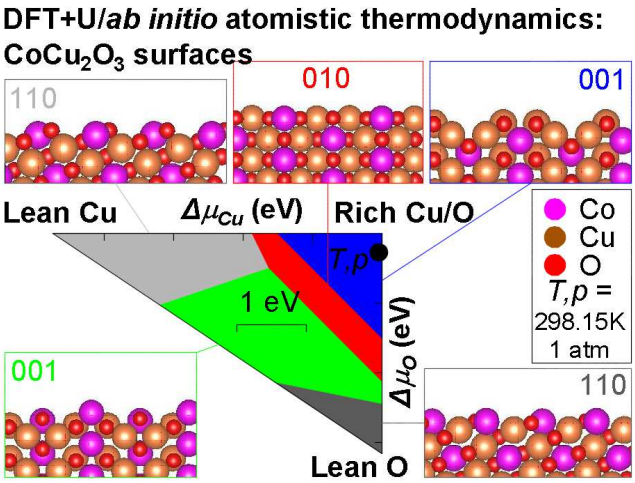

Highlights

- The present study is the first to report DFT + U analysis mixed metallic oxide systems.
- We applied this approach to examine, band gap the structure and relative stability of $CoCu_2O_3$ surfaces.
- This has enabled the determination of thermodynamic stability of respective surfaces.